Ultralight ultrafast enzymes

Xuepei Zhang
Karolinska Institute
Zhaowei Meng
Karolinska Institute
Christian Beusch
Karolinska Institute https://orcid.org/0000-0001-9100-8283
Hassan Gharibi
Karolinska Institute
Qing Cheng
Karolinska Institutet
Luciano Stefano
University of Groningen
Jijing Wang
Karolinska Institute
Amir Saei
Karolinska Institutet https://orcid.org/0000-0002-2639-6328
Akos Vegvari
Karolinska Institute https://orcid.org/0000-0002-1287-0906
Massimiliano Gaetani
Division of Physiological Chemistry I, Department of Medical Biochemistry and Biophysics, Karolinska Institute https://orcid.org/0000-0001-5610-0797
Roman Zubarev (**Roman.Zubarev@ki.se**)
Karolinska Institute https://orcid.org/0000-0001-9839-2089

Article

Keywords: stable isotopes, isotopic ratio, mass spectrometry, isotopic resonance

Posted Date: December 15th, 2021

DOI: https://doi.org/10.21203/rs.3.rs-1103656/v1

Abstract

Inorganic materials depleted of heavy stable isotopes are known to deviate strongly in some physico-chemical properties from their isotopically natural (native) counterparts; however, in biotechnology such effects have not been investigated yet. Here we explored for the first time the effect of simultaneous depletion of the heavy carbon, hydrogen, oxygen and nitrogen isotopes on the bacterium *E. coli* and the enzymes expressed in it. Bacteria showed faster growth, with proteins exhibiting higher thermal stability, while for recombinant enzymes expressed in ultralight media, faster kinetics was discovered. At room temperature, luciferase, thioredoxin and dihydrofolate reductase showed a 40-250% increase in activity compared to the native counterparts. The efficiency of ultralight Pfu DNA polymerase in polymerase chain reaction was also significantly higher than that of the normal enzyme. At 10 °C, the advantage factor of ultralight enzymes typically increased by 50%, which points towards the reduction in structural entropy as the main factor explaining the kinetic effect of heavy isotope depletion. Ultralight enzymes may find an application where extreme reaction rates are required.

Introduction

Isotopes are atoms of the same element that share the same atomic number, but possess different number of neutrons, which is translated in a mass difference. Most elements have several stable isotopes (e.g., carbon has two and oxygen – three stable isotopes), and thus almost all natural compounds have a polyisotopic composition. The question to what extent the isotopic composition plays a role in physical, chemical and biological processes has interested scientists since the discovery of stable isotopes by Aston in 1919. To answer this question best, pure isotopes of different elements have been isolated and studied. The materials and compounds in which the heavier, less abundant isotopes have been significantly depleted are called here ultralight or (near-)monoisotopic. In solid state physics, it has been found that near-monoisotopic materials possess strongly deviating properties: e.g., silicon ^{28}Si (99.87%) has a 60% higher thermal conductivity at 80K than silicon with natural (≈92% ^{28}Si) isotopic composition[1]. Qualitatively similar results have been obtained for monoisotopic diamond (99.8% ^{12}C)[2] and gallium arsenide. Strikingly, the thermal conductivity of germanium enriched to 99.99% ^{70}Ge increased up to 8 times compared to the natural isotopic composition, in which the share of ^{70}Ge among the five stable gallium isotopes is 21.2%[3]. Today, monoisotopic ^{28}Si that is free of nuclear spins causing decoherence in a quantum system emerges as a critical material in the development of quantum information devices, such as quantum computers[3].

On the molecular level, monoisotopic species can exhibit different kinetics of formation than their polyisotopic counterparts. In the reaction of ozone O_3 synthesis from molecular oxygen O_2 by electrical discharge, the isotope effects alter the reaction rates by typically 10% to 20% depending on the pressure and temperature of the gas in which ozone is formed[4]. The strictly monoisotopic isotopomers $^{16}O^{16}O^{16}O$, $^{17}O^{17}O^{17}O$ and $^{18}O^{18}O^{18}O$ have been found to deviate in formation kinetics from other isotopomers, especially the tri-isotopic $^{16}O^{17}O^{18}O$ [5, 6].

In biological systems, each of the four most abundant elements (C, H, O and N) has more than one stable isotope, the lighter one being the most abundant (e.g., the share of ^{12}C is 98.9%). Microbes, plants and animals, including mammals, can grow in an environment with significantly altered ratios of stable isotopes compared to natural, but the phenotype of the organisms can be significantly affected[7-14]. The researchers concluded that the "*organisms of different isotopic compositions are actually different organisms, to the degree that their isotopic compositions are removed from naturally occurring compositions*"[10].

Among the studies in which the heavy isotopes have been depleted, most reported effects relate to deuterium depletion in water. A major deuterium-depleted water (DDW) phenomenon is the depressed growth of cancer cells[15, 16], which is currently being exploited in a clinical trial[17, 18]. Recently, while studying the antiproliferation effect of DDW in human lung adenocarcinoma cells, we found that DDW induces mitochondrial redox imbalance which leads to oxidative stress[19]. In general, deuterium concentration around the natural value of 150 ppm is found to be a cell growth regulator[20].

It is the easiest to manipulate the isotopic composition of bacteria and yeast, as some strains of these can grow on minimal media composed of water, inorganic salts and a simple organic compound (e.g., an amino acid, glucose or carboxylic acid) as a source of carbon. For instance, the effect of depletion of ^{13}C on *E. coli* bacteria growth has been reported[21].

Simultaneous depletion of several heavy stable isotopes in growth media leading to nearly-monoisotopic organisms have been used for decades to produce near-monoisotopic bacterial proteins for structural studies, e.g. with high-resolution mass spectrometry[22, 23]. However, the effect of the ultralight composition on organism's phenotype has not been reported yet to the best of our knowledge. Having acquired considerable experience in measuring the parameters of bacterial growth in various isotopic environments[21, 24-26], we decided to investigate the effect of the depleted media on the growth and phenotype of *E. coli*. For this, we formulated a M9 minimum media based on ^{13}C-depleted glucose and ^{15}N-depleted salt dissolved in D,^{18}O-depleted water (Depleted media). As a control, the growth of *E. coli* in isotopically natural media (Normal media) was monitored. Four different enzymes were recombinantly produced in Depleted as well as Normal media, and their activity was carefully measured. We found much bigger effects than previously reported for isotope phenomena in molecules, including the kinetics of ozone formation.

Results

The growth of E. coli **BL21**. The values of lag time, maximum growth rate and maximum density were used[21] for comparison of the *E. coli* growth in Normal and Depleted media (Fig. 1a). All three parameters indicated that the Depleted media was more beneficial for bacterial growth, providing a significantly (all p-values $<<10^{-6}$, $n = 21$) higher maximum density, faster growth rate as well as a shorter lag time (Fig. 1b).

LC-MS analysis of bacterial lysate showed that in most proteins with MW <20 kDa the monoisotopic mass dominates in the isotopic distribution of molecular ions (Fig. 1c). Fourier Transform Isotopic Ratio Mass spectrometry (FT IsoR MS) of the peptide digest obtained from *E. coli* lysate that is based on the analysis of the "fine structure" of fragment immonium ions of amino acid residues proved deep depletion of ^{13}C, significant depletion of ^{15}N as well as a moderate reduction in deuterium in bacterial proteins (Fig. 1d).

Dose dependence in Depleted media dilution. When the Depleted media was diluted by the Normal media to below 80%, the maximum density of *E. coli* bacteria started to deviate significantly from that in pure Depleted media (Fig. 1e), while maximum growth rate was affected only at a dilution below 40% (Supplementary Fig. 1).

Thermal stability of bacterial proteins. Thermal proteome profiling is rapidly becoming one of the standard methods of proteome analysis[27]. Briefly, the cellular or bacterial lysate undergoes a 3 min incubation at a set of fixed temperature points ranging from 37°C to 83°C, after which the denatured proteins that lost their solubility are spun down and the concentration of each remaining protein in the supernatant is measured by proteomics. The resultant data are fitted with a sigmoidal curve (Fig. 2a), and the middle point provides the melting temperature T_m. When two growth conditions are compared, the melting temperature difference ΔT_m is considered.

The distribution of *E. coli* ΔTm values (Fig. 2b, Supplementary Table 1) reveals that more proteins increase their thermal stability upon becoming ultralight than decrease this stability. The median melting temperature of such proteins was ΔT_m= 1.0±0.1°C higher than that of the proteins obtained in Normal media (Supplementary Fig. 2).

We also noticed that the melting curve of many ultralight proteins shows steeper decline with temperature than their isotopically natural counterparts. To test this observation, the melting curves were fitted with the equation:

$$y = ((1 - Pl) / (1 + \exp((x-T_m)/(B\times x)))) + Pl \quad (1)$$

where the term B is responsible for the slope steepness (lower values mean steeper curve) and Pl is plateau. Of the 316 proteins found with significantly ($p<0.05$) altered slope, 239 proteins (76%) had a steeper slope in the ultralight form (Fig. 2c, Supplementary Table 2). The median slope of ultralight proteins was 27% higher than that of the proteins in Normal media (Fig. 2d).

Luciferase YY5. We expressed recombinantly luciferase YY5[28] in *E. coli* grown in both Normal and Depleted media. In order to ensure validity of the comparison, a single peak in size-exclusion chromatography (SEC) was isolated (Supplementary Fig. 3a) possessing activity. However, mass spectrometry (MS) analysis showed that the isolated peak contains at least two molecules with different molecular weights. Therefore, an additional purification step using strong cation exchange (SCX) chromatography was implemented, which gave two well-separated fractions, fracI and fracII

(Supplementary Fig. 2b). Both fractions, especially fracII, showed strong luciferase activity, and MS analysis confirmed that fracII contains just one molecular specie. Tandem MS analysis of that fraction provided isotopic distribution of the y_{87}^{12+} backbone fragment, with the monoisotopic mass dominant in the Ultralight sample, consistent with strong depletion of heavy isotopes in that sample (Fig. 3a). Charge deconvolution provided the average isotopic molecular mass of 61,728.9±0.3 Da of the Normal luciferase in fracII, which was by 240.8±0.3 Da higher than expected (Supplementary Fig. 3e). The difference was attributed to a combination of biotinylation and methylation, which are common post-translational modifications (PTMs) in recombinant proteins[29]. The Ultralight fracII sample gave the average isotopic mass of 61,697.5±0.3 Da, or 7.6±0.4 Da higher than the expected monoisotopic mass given the 240.8±0.3 Da mass shift due to a combination of biotinylation and methylation (Supplementary Fig. 3e). Since in the Normal sample, the expected isotopic shift (the difference between the average isotopic and monoisotopic masses)[30] is 39.0 Da, the heavy isotopes in the Ultralight luciferase were depleted on average by 81%:

Depletion% = [average MW (Normal - Ultralight)]/Isotopic shift ×100 (2)

The activity of fraction fracII was measured for different concentrations of the substrate D-luciferin (Fig. 3b). The fitted Michaelis-Menten equation provided the Vmax and Km values. The maximum reaction rate Vmax of the Ultralight luciferase was found to be 2.5±0.2 higher than the Normal one ($P=3\cdot10^{-7}$, $n=4$), while the K_m value (Michaelis constant, numerically equal to the substrate concentration at which the reaction rate is half of Vmax) was not significantly changed. The activity of the Depleted luciferase YY5 started to decline significantly when the Depleted media was diluted by the Normal media to below 80% (Fig. 3d), which was a similar effect to that observed for *E. coli* growth parameters (Fig. 1e).

The fraction fracI turned out to be somewhat heterogeneous, with the main component corresponding to a combination of double biotinylation and methylation (Supplementary Fig. 3c and 3d). This fraction showed an order of magnitude lower activity than fracII (Supplementary Fig. 3f and 3g). It also demonstrated a significant Ultralight/Normal ratio in maximum reaction rate (1.7±0.2, $P=2\times10^{-5}$), and a small reduction in K_m (0.87±0.05, P=0.02) (Supplementary Fig. 3h).

To test the refolding ability of the enzyme after thermal unfolding, the fracII luciferase samples were incubated at 50°C for up to 100 min and then cooled down to RT. As expected, the enzyme activity has dropped, but at all tested time points, the Ultralight enzyme demonstrated a 1.6±0.1 times higher activity than the Normal enzyme (Fig. 3e). Importantly, at lower temperature than RT the ratio of Ultralight/Normal activity for untreated fracII enzyme was increasing, reaching 2.3±0.1 times at 10°C (Fig. 3f).

Thioredoxin. Another tested enzyme was thioredoxin (Trx), an oxidation-reduction active enzyme containing a cystine disulfide that is reduced to the dithiol cysteine form by thioredoxin reductase (TrxR) with NADPH as a cofactor[31]. The reduced Trx can oxidize again by reducing its substrate, such as insulin that is composed of peptide chains A and B linked together by two disulfide bonds. Reduction of insulin in solution results in white precipitation originating from the free B chain, which is used for measuring Trx

activity. Trx (Supplementary Fig. 4a-c) was expressed recombinantly in *E. coli* grown in both Normal and Depleted media, purified and quantified by SEC (Supplementary Fig. 4d), with the purity verified by mass spectrometry (Fig. 4a). Monoisotopic mass dominates in the isotopic distribution of molecular ions in the Ultralight sample, which proved strong depletion of the heavy isotopes in that sample (Supplementary Fig. 4e). The monoisotopic mass of the Ultralight protein was 11,784.9±0.1 Da, which was by 1.9±0.1 Da lower than expected. The difference was attributed to a disulfide linkage between two cysteine residues, which is a frequent post-translational modification in recombinant proteins [32]. The depletion of Ultralight Trx was 65%.

The activity of thioredoxin was measured for different concentrations of the substrate insulin (Fig. 4c) by fitting the Michaelis-Menten equation (Fig. 4d). The maximum reaction rate of the Ultralight thioredoxin was found to be (17±1)% higher than the Normal one (P=0.002, n=3), while the K_m value was not significantly altered.

The activity of enzyme was also measured at different temperatures in the range 15-40°C. As expected, the enzyme activity dropped at lower temperature, but the Ultralight/Normal activity ratio increased to 2.0±0.3 at 15°C (Fig. 4e).

Dihydrofolate reductase. Dihydrofolate Reductase (DHFR) is a ubiquitous enzyme that is present in all eukaryotic and prokaryotic cells. DHFR catalyzes the transfer of a hydride from NADPH to dihydrofolate with an accompanying protonation to produce tetrahydrofolate, during which NADPH is oxidized to $NADP^+$. By monitoring the decrease in absorbance at 340 nm, at which NADPH has specific absorbance, the ability of DHFR to catalyze the oxidation of NADPH can be measured. DHFR from *Geobacillus stearothermophilus* (BsDHFR, Supplementary Fig. 5a and 5b) was expressed recombinantly in *E. coli* grown in both Normal and Depleted media, purified and quantified by SEC (Supplementary Fig. 5c), with the purity verified by mass spectrometry (Fig. 5a). Monoisotopic mass dominates in the isotopic distribution of molecular ions in the Ultralight sample, while charge and isotope deconvolution of the Normal BsDHFR mass spectrum provided the average molecular mass of 33820.4±0.2 Da, which was only 0.2 Da lower than expected and within the experimental error. The average mass of the Ultralight protein revealed the isotopic shift of 5.0±0.2 Da (Supplementary Fig. 5d), consistent with the depletion degree of 76%.

The activity of BsDHFR was measured in the presence of 200 μM DHF and 100 μM NADPH. The decrease in 340 nm UV absorbance for the reaction catalyzed by Ultralight BsDHFR was significantly faster compared with the Normal enzyme (Fig. 5b), which was reflected in a steeper decreasing curve for Ultralight BsDHFR. The fitted Michaelis-Menten equation (Fig. 5c) revealed a (70±2)% higher maximum reaction rate for Depleted vs Normal BsDHFR ($P=10^{-5}$, n=4), while the K_m value was again not significantly changed.

Similar to other tested enzymes, the activity of BsDHFR measured in the range 10-30°C dropped at lower temperature, but the Ultralight/Normal activity ratio increased, reaching 2.1±0.2 at 10°C (Fig. 5e).

Pfu DNA polymerase. Polymerase chain reaction (PCR) proved to be one of the biggest revolutions in molecular biology. Due to its extremely high sensitivity and dynamic range, the potential for high throughout as well as semi-quantitative nature, PCR is now widely used in research, clinical diagnostics, etc. [33] For example, viral nucleic acid detection by real time (RT)–PCR remains the gold standard of current diagnostic tests for the SARS-CoV-2 infection[34]. Although PCR is a mature technology, research is still ongoing to obtain more efficient and DNA polymerase less prone to sequence errors[35]. Pfu DNA polymerase[36] is a high-fidelity, thermostable enzyme isolated from *Pyrococcus furiosus*. In this study, Pfu was expressed recombinantly in *E. coli* grown in both Normal and Depleted media, purified and quantified by SEC (Supplementary Fig. 6a), with the purity verified by mass spectrometry (Fig. 6a). In the Ultralight sample, monoisotopic mass dominates in the isotopic distribution of b_{99}^{20+} ions, which confirms strong depletion of heavy isotopes (Fig. 6a). Charge deconvolution of the Normal Pfu yielded the average isotopic molecular mass of 100,194.3±0.6 Da, which was by 43.4±0.6 Da higher than expected (Supplementary Fig. 6b). The difference was attributed to acetylation, possibly combination with deamidation, which both are common PTMs in recombinant proteins[29]. Taking this into account, the Ultralight sample (Supplementary Fig. 6b) gave the isotopic shift of 12.1±0.6 Da, which corresponds to the depletion degree of 81%.

Human glyceraldehyde-3-phosphate dehydrogenase (GAPDH), one the most used reference genes in RT-PCR assays [37], was selected as the targeted gene for activity assay. RNAs extracted from human non-small lung cancer cell line A549 cells was reverse transcribed to cDNAs which were used as templates for RT-PCR. With the concentration of input cDNAs 2 ng per 20 µL reaction it was found that RT-PCR catalyzed by Ultralight Pfu was significantly faster compared to Normal enzyme (Fig. 6b). ´The cycle threshold (Ct) value for RT-PCR was 11.1±0.3 cycles with Ultralight Pfu, while with Normal Pfu it was 13.6±0.4 cycles (Fig. 6d), consistent with faster kinetics of the Ultralight enzyme. The same qualitatively result was obtained at a lower concentration of cDNA (0.2 ng / 20 µL reaction, Fig. 6c), with Ct values 14.4±0.4 cycles for RT- Ultralight Pfu and 17.1±0.3 cycles for the Normal enzyme (Fig. 6e). The efficiency of PCR with the Ultralight enzyme was significantly higher, (97.7±0.8)%, compared to the Normal enzyme, (92.8±2)% (Fig. 6f). Moreover, the amount of final product in the reaction with the Ultralight enzyme was higher than that in the reaction with the Normal enzyme, which was possibly caused by the lower efficiency of the Normal Pfu.

The activity of Pfu enzyme at different extension temperatures in the range 60-72 ^{o}C was studied by detection of the fluorescence intensity of SYBR green I which presented the amount of double-stranded DNA (dsDNA) produced in PCR. As expected, the enzyme activity dropped at lower temperature (Supplementary Fig. 6c), but the Ultralight/Normal activity ratio increased, with a (54 ±5)% higher activity for Ultralight enzyme at 60°C (Fig. 6g).

Discussion

The most important finding of this work is that at least some enzymes expressed in *E. coli* grown in the Depleted media show faster kinetics than the identical enzymes produced in the Normal media. This finding is further supported by the faster *E. coli* growth in the Depleted media, which necessitates faster (on average) enzymatic activity in the growing organism. The size of the heavy isotope depletion effect is large (≈2.5-fold for luciferase and at least 50% for other enzymes). It should be noted that the isotope depletion, however large in relative terms (>5-fold), is miniscule on the absolute scale, as the natural abundance of the most abundant depleted isotope, ^{13}C, is only 1.1%. Thus the kinetics enhancement due to the normal kinetic isotope effect in strictly monoisotopic enzymes should be <1%. This reasoning is supported by only a 13% reduction in the reaction speed of the DHFR enzyme with fully substituted heavy isotopes of ^{13}C, ^{15}N and ^{2}H at 40°C [38] and a 40% reduction at 5°C [39]. The kinetics acceleration by up to 250% in Ultralight proteins cannot be accounted by the conventional kinetic isotope effect, and the low P-values obtained ($P=3\cdot10^{-7}$ for luciferase and $P<10^{-11}$ for the combined results of four enzymes) greatly exceeds the five-sigma requirement for new discovery accepted in Physics, not to mention the proposed P<0.005 threshold for discoveries in Life Sciences [40]. Importantly, the majority of the Ultralight enzymes are more thermally stable than Normal enzymes, and the superior kinetics of the Ultralight enzymes is preserved even at higher temperatures.

A simple rationalization of the effect of ultralight enzymes is the following. Due to the dominance in nature of light isotopes, every carbon atom is most likely ^{12}C, every oxygen atom is most likely ^{16}O, etc. As the amino acid sequences of most enzymes are tightly optimized for function by natural selection, the most likely configuration of a native enzyme should have close to maximum activity. Any deviation from that configuration, such as those arising due to heavy isotopic substitution, is likely reducing this optimal activity, however slightly. This qualitative reasoning explains why monoisotopic enzymes should have close to maximum activity for a given amino acid sequence.

For a more involved and potentially quantitative explanation of this phenomenon, we considered the role of entropy in the magic of enzymatic action, which is the enormous rate enhancement achieved by enzymes compared to the equivalent enzyme-free reactions. This role has been debated for over a century, and the debates are still ongoing[41, 42]. There are several well-documented cases where the activation free energy decreases due to enzyme's entropic effects by around 10 kcal/mol, leading to a rate enhancement of $\sim10^{7}$ compared to the uncatalyzed reaction. However, despite substantial experimental and theoretical efforts, there is no real consensus on the origin of such large entropic contributions. Recent efforts have shown that the entropy considerations should not be limited to the substrate entropies alone, but must also include all the relevant activation entropy parts, encompassing the whole protein and its surrounding solvent [41]. The presence of heavy isotopes contributes significantly to the informational protein entropy, with the monoisotopic molecules having the lowest entropy [43]. Indeed, a single ^{13}C atom in a protein molecule containing 10,000 carbon atoms (as in a ≈70 kDa enzyme) will have 10,000 different places to reside in, which immediately results in 10,000 distinct isotopomers. At a 1.1% abundance, there will on average be ca. 110 ^{13}C atoms in such a molecule, giving a very large number of isotopologues [44] differing from each other by the number of ^{13}C atoms. With ^{2}H, ^{15}N, ^{17}O and

^{18}O atoms present, each isotopologue will have an astronomical number of isotopomers [45]. As each protein isotopomer will have its own spectrum of vibrational frequencies distinctly different from other isotopomers [46], vibrational entropy of a poly-isotopic protein could greatly exceed that of the corresponding monoisotopic molecule or of a ultralight protein with much fewer heavy isotopes than natural molecule. Vibrational entropy is known to account for the stability of short alpha-helices[47] and contributes significantly to the stability of globular proteins[48]. In general, vibrations of proteins, especially those local to the active site, play a significant role in the enzymatic activity[49]. Thus it stands to reason that the protein molecules with much lower vibrational entropy, such as monoisotopic or ultralight enzymes, will exhibit significantly altered kinetic parameters than the same enzymes with natural isotopes.

The lower intrinsic entropy due to the isotope depletion can also affect the rates of the protein thermal unfolding and refolding [50]. The thermal profiling experiments performed here on *E. coli* lysate suggested that the majority of proteins increased their measured melting temperature, which could be due to a number of scenarios. One possibility is a combination of an unchanged or slightly increased unfolding rate with faster refolding. In favor of the latter scenario, for the same number of amino acid residues the proteins with lower conformational entropy tend to fold faster [50].

Among other entropy-related explanations of the observed effects is the Isotopic Resonance (IsoRes) phenomenon [21, 24, 25]. Being a generalization of the ideas of Gao and Marcus, the IsoRes paradigm predicts every type of symmetry (defined as a condition leading to a reduction in the number of quantum-mechanical states compared to an asymmetric case) to affect reaction kinetics. At certain isotopic compositions, often corresponding to significant heavy isotope *enrichments* compared to natural isotopic abundances, IsoRes predicted faster kinetics, which has indeed been observed experimentally [21]. The strongest kinetic effect is however predicted by IsoRes for monoisotopic systems, in agreement with the above observations.

Methods

Media Preparation

M9 minimum media were prepared as follows. $Na_2HPO_4.2H_2O$, KH_2PO_4, NaCl, NH_4Cl, $MgSO_4$, $CaCl_2$ and glucose were obtained from Sigma-Aldrich. ^{13}C-depleted glucose was purchased from Cambridge Isotope Laboratories and ^{15}N-depleted $(NH_4)_2SO_4$ was from Merck. Deuterium Depleted Water (DDW) containing ≤5 ppm D and 410 ppm ^{18}O was obtained from MTC Iceberg Ltd (Moscow, Russia). M9 stock salt solutions (M9 5×SS) were prepared by dissolving 42.5 g $Na_2HPO_4.2H_2O$, 15.0 g of KH_2PO_4 and 2.5 g of NaCl in 1000 mL of either normal milli-Q water (for Normal M9 media) or DDW (for Depleted M9 media). Both solutions were autoclaved before proceeding to M9 media preparation. M9 media were prepared by mixing 800 mL of either normal milli-Q water (for Normal M9 media) or DDW (for Depleted M9 media), 200 mL of the corresponding M9 5xSS, 2.0 mL of 1M $MgSO_4$, 0.1 mL of 1M $CaCl_2$, 5 g of glucose and 1 g

of $(NH_4)_2SO_4$ (isotopically normal for Normal M9 media and ^{13}C-depleted glucose and ^{15}N-depleted $(NH_4)_2SO_4$ for Depleted M9 media). These media were filtered using 0.2 µm polyether sulfone (PES) filters (VWR) before use.

E. coli **growth**

For each set of experiments, *E. coli* BL 21 strain was grown on plates containing LB agar (Sigma). A single colony was transferred to a tube containing 6 mL of Normal M9 media and grown for 36 h. These bacteria were further diluted (1:500) into tubes containing either Normal or Depleted M9 media and put into honeycomb well plates (BioScreen, Finland) in 21 replicates. Bacterial growth was monitored by measuring light diffraction on a BioScreen C instrument (BioScreen, Finland) at 37°C.

TPP sample preparation

E. coli BL21 grown in Normal and Depleted M9 media were diluted (1:500) into tubes containing either Normal or Depleted M9 media in flasks. After 36 h of growth, the bacteria in each flask were collected, washed, resuspended in PBS with protease inhibitor (5892791001, Sigma) and lysed by probe sonication. The protein solution was collected after centrifuge and divided into 8 aliquots. These aliquots were incubated for 3 min at either 37, 43, 49, 55, 61, 67, 73 or 79°C. After that the samples were kept at RT for 5 min to cool down and ultra-centrifuged at 35,000 rpm/min at 4°C for 30 min. Afterwards, the supernatant was collected, reduced with 10 mM DTT (10708984001, Sigma) and alkylated with 25 mM IAA (I1149, Sigma). The samples were precipitated using cold acetone at -20°C overnight, digested by Lys C (125–05061, Wako Chemicals GmbH) at a 1:75 enzyme to protein ratio for 6 h at 30°C and then by trypsin (V5111, Promega) (1:50 enzyme to protein ratio) overnight. After labeling using 16 TMTpro reagents (A44520, Thermo Fisher Scientific) according to manufacturer's instructions, multiplexing and desalting with C18 Sep-pak columns (WAT054960, Waters), the peptides samples were fractionated using a Dionex Ultimate 3000 UPLC system (Thermo Fisher Scientific) as described before [20]. Every 8 fractions were combined to a single pool and 12 such pools for each TMT-multiplexed sample set were analyzed by nanoLC-MS/MS as customary in shotgun proteomics.

NanoLC-MS/MS analysis

NanoLC-MS/MS analyses were performed on an Orbitrap Fusion Lumos mass spectrometer (Thermo Fisher Scientific). The instrument was equipped with an EASY ElectroSpray source and connected online to an Ultimate 3000 nanoflow UPLC system. The samples were pre-concentrated and desalted online using a PepMap C18 nano-trap column (length - 2 cm; inner diameter - 75 µm; particle size - 3 µm; pore size - 100 Å; Thermo Fisher Scientific) with a flow rate of 3 µL/min for 5 min. Peptide separation was performed on an EASY-Spray C18 reversed-phase nano-LC column (Acclaim PepMap RSLC; length - 50 cm; inner diameter - 2 µm; particle size - 2 µm; pore size – 100 Å; Thermo Scientific) at 55 °C and a flow rate of 300 nL/min. Peptides were separated using a binary solvent system consisting of 0.1% (v/v) FA, 2% (v/v) ACN (solvent A) and 98% ACN (v/v), 0.1% (v/v) FA (solvent B). They were eluted with a gradient of 3–26% B in 97 min, and 26–95% B in 9 min. Subsequently, the analytical column was washed with

95% B for 5 min before re-equilibration with 3% B. The mass spectrometer was operated in a data-dependent acquisition mode. A survey mass spectrum (from m/z 375 to 1500) was acquired in the Orbitrap analyzer at a nominal resolution of 120,000. The automatic gain control (AGC) target for was set as 100% standard, with the maximum injection time of 50 ms. The most abundant ions in charge states 2^+ to 7^+ were isolated in a 3 s cycle, fragmented using HCD MS/MS with 33% normalized collision energy, and detected in the Orbitrap analyzer at a nominal mass resolution of 50,000. The AGC target for MS/MS was set as 250% standard with a maximum injection time of 100 ms, whereas dynamic exclusion was set to 45 s with a 10-ppm mass window.

Expression and purification of luciferase YY5

Part of this work was performed by the Protein Science Facility at Karolinska Institutet, Stockholm. The construct psfLucYY5 was transformed into *E. coli* BL21 (DE3) T1R pRARE2 cells in Normal and Depleted M9 media containing 50 µg/mL ampicillin and 34 µg/mL chloramphenicol at 37°C. The bacterial growth was monitored by regular OD measurements. Protein expression of the fusion proteins was induced by the addition of 0.5 mM isopropyl-1-thio-β-D-galactopyranoside (IPTG, Merck). The cells were harvested after 16 h by centrifugation, and the pellet was resuspended in lysis buffer including 100 mM HEPES, 500 mM NaCl, 10% glycerol, 10 mM imidazole, 0.5 mM TCEP, pH 8.0, 1 mg/mL lysozyme, 0.1% DDM, 1 mM $MgSO_4$, protease inhibitors (complete EDTA-free 0.5 tab/mL), and benzonase (0.125 U/mL). After centrifugation, the samples were loaded onto a resin column (GE Healthcare) equilibrated with binding buffer (20 mM HEPES, 500 mM NaCl, 10% glycerol, 10 mM imidazole and 0.5 mM TCEP, at pH 7.5). The column was washed with binding buffer followed by washing buffer (same as binding buffer but with 30 mM imidazole), and then recombinant luciferase YY5 was eluted with a similar buffer containing 500 mM imidazole. Fractions containing luciferase YY5 were combined and applied to a PD 10 column (GE Healthcare) equilibrated with 50 mM Tris-HCl at pH 7.8. The size and purity of recombinant luciferase YY5 was confirmed by SDS-PAGE.

Expression and purification of human Trx

The Trx expression plasmid (Supplementary Fig. 3a-c) was transformed into *E. coli* BL21 (DE) in Normal and Depleted M9 media containing 50 µg/mL kanamycin (Merck, K1377) and the expression and purification of Trx was performed as described above. Fractions containing Trx according to SDS-PAGE analysis were pooled together and TEV protease (Sigma) was added to the protein sample at a 1:30 molar ratio. The mixture was incubated at 4°C overnight. The His-tag was removed by loading the protein sample onto a 1 mL HisTrap column (GE Healthcare) pre-equilibrated with TEV cleavage reaction buffer supplemented with 20 mM imidazole. The flow-through containing cleaved Trx protein was collected and the purification fractions were analyzed by SDS-PAGE.

Expression and purification of BsDHFR

The BsDHFR expression plasmid (Supplementary Fig. 4a and 4b) was transformed into *E. coli* BL21 (DE) in Normal and Depleted M9 media containing 50 µg/mL kanamycin and the expression and purification

of BsDHFR was performed as above.

Expression and purification of Pfu

The construct Pfu DNA polymerase with Sso7d processivity-enhancing domain was transformed into *E. coli* BL21 (DE3) T1R cells in Normal and Depleted M9 media containing 50 µg/mL ampicillin and 34 µg/mL chloramphenicol. The expression and purification of BsDHFR was performed as above.

Size exclusion chromatography (SEC)

SEC purification of the recombinant proteins was performed on a Dionex Ultimate 3000 UPLC system (Thermo Fisher Scientific) with a 25 cm Waters column (2.1 mm ID; particle size 3.5 µm; pore size 300 Å) at a flow rate of 300 µL/min. Fractionation of luciferase YY5, BsDHFR and Pfu were performed using 2× phosphate-buffered saline diluted from 10× PBS (Lonza, 17517Q). Trx was purified using 50mM Tris-HCl at pH 7.5 containing 2 mM EDTA. The elution was monitored by UV absorbance at 280 and 214 nm.

Strong cation exchange (SCX) chromatography

Luciferase YY5 isolated with SEC was additionally purified by SCX using a Dionex Ultimate 3000 UPLC system (Thermo Fisher Scientific) with ProPac Strong Cation-Exchange Column (4×250mm, Thermo Fisher Scientific) at a flow rate of 500 µL/min. Fractionation was performed using a binary solvent system consisting of 12.5 mM sodium phosphate, pH 6.0 (solvent A) and 12.5 mM sodium phosphate, 1 M NaCl, pH 6.0 (solvent B). Elution was done with a 30 min gradient from 1–58% B monitored by UV absorbance at 280 nm. Two fractions showing luciferase activity were collected and used for further analysis.

Measurements of luciferase YY5 activity

Buffered co-factor solution (8 mL) was prepared containing 1 mM DTT, 0.2 mg/mL BSA, 5 mM of $MgCl_2$, 4 mM DTT, 100 µM $_D$-luciferin and 100 mM Tris-HCl at pH 7.8. 50 µL of each SCX fraction was mixed with 50 µL buffered co-factor solution in a 96-well microplate well and the luminescence was measured using the Tecan Infinite M2000 PRO microplate reader. The luminescence of each fraction was normalized by the total 280 nm UV absorbance of the SCX fraction.

Thermal stability assay of luciferase YY5

The protein concentration of Normal and Ultralight SEC-SCX purified luciferase YY5 was determined by microBCA and 50 µL of 0.2 µg/mL enzyme was heated at 50°C for 5-120 min. After cooling to RT, the enzyme solution was mixed with 50 µL of the reaction buffer containing 1 mM DTT, 0.2 mg/mL BSA, 5 mM of $MgSO_4$, 4 mM DTT, 100 µM $_D$-luciferin and 100 mM Tris–HCl at pH 7.8. The luciferase activity was measured at 25°C using the Tecan Infinite M2000 PRO microplate reader.

Measurement of Trx activity

The assay was performed at RT using 50 mM Tris-HCl containing 2 mM EDTA at pH 7.5 and 200 μM NADPH (Roche, 10107824001). A 60 μL aliquot of each Trx SEC fraction was mixed in a 96-well microplate well with 30 μL buffered enzyme solution containing 15 nM thioredoxin reductase and 10 μL of insulin (Sigma, I0516) at a concentration ranging from 0 to 160 μM (the latter corresponds to 1 mg/mL). NADPH consumption was measured immediately every minute by the decrease of absorbance at 340 nm during the initial linear phase of reaction in the Tecan Infinite M2000 PRO microplate reader. The magnitude of the absorbance decrease at 340 nm of each fraction was normalized by the total UV absorbance at 280 nm of the Trx SEC fraction.

Measurement of BsDHFR activity

The assay was performed at RT using 50 mM Tris-HCl at pH 7.5. A 60 μL aliquot of each BsDHFR SEC fraction was mixed in a 96-well microplate well with 30 μL buffered enzyme solution containing 200 μM dihydrofolic acid (Merck, D7006). NADPH consumption was measured immediately by the decrease of absorbance at 340 after a concentration ranging from 0 to 100 μM NADPH was added.

PCR and RT-PCR catalyzed by recombinant Pfu

RNA was extracted from 10^7 A549 cells and purified using a PureLink RNA Mini Kit (Thermo Fisher Scientific, 12183018A). A cDNA library was prepared using the High-Capacity cDNA Reverse Transcription Kit with RNase Inhibitor (Thermo Fisher Scientific, 4374966) according to manufacturer's instructions. RT-PCR and PCR were performed with 0-2 μg cDNA in 20 mM Tris-HCl containing 50 mM KCl, 10 mM $(NH_4)SO_4$, 2 mM Triton X-100 and 0.1 mg/mL BSA (PCR buffer) at pH 8.8 with 0.2 mM dNTP (Thermo Fisher Scientific, N8080261), and 1 X SYBR green I (Thermo Fisher Scientific, 10710004). Human gene GAPDH (10 μM, 131 bp) was used in the assay and the sequences of the primers were: 5' to 3' GTCTCCTCTGACTTCAACAGCG (Forward) and 5' to 3' ACCACCCTGTTGCTGTAGCCAA (Reversed) (Thermo Fisher Scientific). Normal or Ultralight Pfu purified by SEC was diluted with PCR buffer to 30 ng/mL and 1 mL was added to each 20 μL reaction volume. The PCR program on SimpliAmp Thermal Cycler (Thermo Fisher Scientific) was 98°C for 2 min → 98°C for 10 s → 56°C for 30 s → 72°C for 30 s for 34 cycles and keep the reaction at 72°C for 5 min. RT-PCR was performed on Applied Biosystems Fast 7500 (Thermo Fisher Scientific) using the same program as PCR.

The gel for agarose gel electrophoresis was prepared by suspending 1 Advance Agarose Tablet (Genetics, AG11) in 50 mL TBE buffer (89 mM Tris-borate and 2 mM EDTA, pH 8.3). each PCR final solution was mixed with 2 μL FastDigest Green Buffer (Thermo Fisher Scientific, B72) and 15 μL mixture was loaded in the gel. Then the gel was run at 80-150 V until the dye line reached ca. 75-80% of the gel length. Afterwards, the DNA fragment was visualized under UV light at 280 nm.

Bottom-up proteomics data analysis

The LC-MS/MS raw files were processed by an in-house modified version of MaxQuant software (version 1.6.2.3) recognizing TMTpro as an isobaric mass tag using the "Specific Trypsin/P, Lyc/P" digestion

mode with maximum two missed cleavages as described before [20]. The MS/MS spectra were searched against the Uniprot *Escherichia coli* BL21 database (UP000290528, containing 4,339 entries, last modified on January 6, 2020).

Top-down mass spectrometry analysis analysis

The SEC or SCX fractions were concentrated using a 3 kDa centrifugal filter (Merck, UFC500324). The proteins were desalted using ZipTip with 0.6 µL C_4 resin (Merck, ZTC04S096). On-line LC-MS/MS analysis was performed using a Dionex Ultimate NCS-3500RS Nano System coupled to an Orbitrap Fusion Lumos mass spectrometer equipped with a HESI Ion Source (all – Thermo Fisher Scientific).

Protein separation online with MS was performed using a C_4 reversed-phase PepMap™ 300 micro-flow HPLC column (particle size 5 µm, 1 mm ID × 15 cm, Thermo Fisher Scientific) enclosed in a column oven compartment maintained at 45°C, at a flow rate of 30 µL/min. 1 µg of protein sample was loaded and separated using a binary solvent system consisting of Solvent A (2% acetonitrile, 98% water and 0.1% formic acid) and Solvent B (2% water, 98% acetonitrile and 0.1% formic acid). The mobile phase composition was 5% B from 0 to 2 min, followed by a 5-30% B gradient from 2 to 5 min, 30-95% B from 5 to 25 min, 95-5% B from 34 to 35 min and 5% B from 35 to 40 min. The electrospray voltage was 3.7 kV with sheath gas at 15 units, auxiliary gas at 5 units and the vaporizer temperature at 75°C. The capillary temperature was set at 300°C. The RF lens amplitude was set at 30% and an additional 15 V voltage difference was applied within the source region to facilitate ion desolvation. All mass spectra were acquired in the positive ion mode with the profile data type. Application mode was set at “intact protein” with the collision gas pressure 1 mTorr. The nominal mass resolution at m/z 200 for luciferase and Pfu was 15,000, for Trx and BsDHFR - 120,000, with 200% Normalized AGC and 10 microscans over a mass range of m/z 500-1500. For tandem mass spectrometry, the most abundant charge states of the protein ions were selected in a quadrupole mass filter with isolation window of 3.0 m/z units for higher-energy collision dissociation (HCD) with normalized collision energy set at 20%. The range of charge states was 10-100 with the underdetermined charge states included. The MS/MS spectra were acquired with 3 dependent MS/MS events with a nominal mass resolving power of 120,000 with 5 microscans, over a mass range of m/z 400-2000, with 500% Normalized AGC Target and Auto Maximum Injection Time. The Dynamic exclusion was operated with exclusion duration of 30 s, mass width (High/Low) of 1.5 m/z units and the repeat count set at 1. All mass spectra were analyzed, including isotope and charge deconvolution, using Xcalibur 4.3 (Thermo Fisher Scientific) and the Average Over Selected Retention Time and ReSpect™ (Isotopically Unresolved for luciferase YY5 and Pfu, Isotopically Resolved for Trx and BsDHFR) algorithms in Thermo Scientific™ BioPharma Finder™ 2.0 software. Protein mass tolerance was set to 20 ppm, and data were searched against the known protein amino acid sequence, allowing for amidation (DE, C-term), acetylation (N-term), biotinylation (K), methylation (KR), oxidation (MW) and deamidation (NQ) as variable modifications.

FT IsoR MS analysis

Bacterial lysate was digested as above, and after desalting the peptides were analyzed by nanoLC-MS/MS. Mass spectra were acquired on an Orbitrap Fusion Lumos Mass in the data-independent mode with z≥2 peptides selected for MS/MS in an isolation window 1000 m/z units wide centered at m/z 800. MS/MS was performed with HCD energy set at 50 NCE. The detection range was from m/z 50 to 200, with the nominal mass resolving power of 60,000. Data processing was done using a home-written R script analyzing the fine isotopic structure of the immonium ions of amino acids Pro, Val and Leu/Ile.

Declarations

Acknowledgements

This work was funded by the Swedish Research Council. Yokobayashi lab in Okinawa Institute of Science and Technology Graduate University, Japan is acknowledged for providing a construct of firefly luciferase. Protein Science Facility at Karolinska Institutet, Stockholm is acknowledged for expression and purification of recombinant enzymes. R.A.Z acknowledges support from The Ministry of Science and Higher Education of the Russian Federation (agreement no. 075-15-2020-899). A.A.S. was supported by Swedish Research Council (grant 2020-00687) and the Swedish Society of Medicine (grant SLS-961262, 1086 Stiftelsen Albert Nilssons forskningsfond).

Author contributions

R.A.Z. conceived the project and supervised the study. R.A.Z. and X.Z. designed the experiments. X.Z. performed enzyme activity assay, thermal proteome profiling and FT IsoR MS. X.Z. and Z.M. performed the purification and MS analysis of recombinant enzymes. C.M.B. analyzed the thermal proteome profiling data. H.G. analyzed FT IsoR MS data. X.Z. and Q.C. performed expression and purification of luciferase YY5, Trx and BsDHFR. X.Z. and L.DS. performed growth of *E.coli* in different media. J.W., A.A.S., Á.V. and M.G. discussed the results and provided support for experimental design, instrumental resources and technical solutions. R.A.Z. and X.Z. wrote the manuscript. All authors approved the final version of the manuscript.

Competing interests

The authors declare no competing interests.

References

1. Ruf, T. et al. Thermal conductivity of isotopically enriched silicon. *Solid State Commun.* **115**, 243–247 (2000).
2. Anthony, T.R. et al. Thermal diffusivity of isotopically enriched ^{12}C diamond. *Physical Review B* **42**, 1104–1111 (1990).
3. Ozhogin, V.I. et al. Isotope effect in the thermal conductivity of germanium single crystals. *JETP Letters* **63**, 490–494 (1996).

4. III, J.E.H. & Thiemens, M.H. A non-mass-dependent oxygen isotope effect in the production of ozone from molecular oxygen: The role of molecular symmetry in isotope chemistry. *J. Chem. Phys.* **84**, 2129–2136 (1986).
5. Krankowsky, D. & Mauersberger, K. Heavy Ozone--A Difficult Puzzle to Solve. *Science* **274**, 1324–1325 (1996).
6. Michalski, G. & Bhattacharya, S.K. The role of symmetry in the mass independent isotope effect in ozone. *Proc. Natl. Acad. Sci. U.S.A.* **106**, 5493-5496 (2009).
7. Katz, J.J., Crespi, H.L., Hasterlik, R.J., Thomson, J.F. & Finkel, A.J. Some observations on biological effects of deuterium, with special reference to effects on neoplastic processes. *J. Natl. Cancer Inst.* **18**, 641–659 (1957).
8. Borek, E. & Rittenberg, D. Anomalous growth of microorganisms produced by changes in isotopes in their environment. *Proc. Natl. Acad. Sci. U. S. A.* **46**, 777-782 (1960).
9. Katz, J.J. & Crespi, H.L. Deuterated organisms: cultivation and uses. *Science* **151**, 1187–1194 (1966).
10. Uphaus, R.A., Flaumenhaft, E. & Katz, J.J. A living organism of unusual isotopic composition. Sequential and cumulative replacement of stable isotopes in Chlorella vulgaris. *Biochim. Biophys. Acta* **141**, 625–632 (1967).
11. Rokop, S., Gajda, L., Parmerter, S., Crespi, H.L. & Katz, J.J. Purification and characterization of fully deuterated enzymes. *Biochimica et Biophysica Acta (BBA) - Enzymology* **191**, 707–715 (1969).
12. Katz JJ, C.H. in Isotope effects in chemical reactions. (ed. C.J. Collins, Bowman NS) 86–363 (Van Nostrand Reinhold, New York; 1971).
13. Fowler, E.B., Adams, W.H., Christenson, C.W., Kollman, V.H. & Buchholz, J.R. Kinetic studies of C. pyrenoidosa using 94% 13C CO2. *Biotechnol. Bioeng.* **14**, 819–829 (1972).
14. Paliy, O., Bloor, D., Brockwell, D., Gilbert, P. & Barber, J. Improved methods of cultivation and production of deuteriated proteins from E. coli strains grown on fully deuteriated minimal medium. *J. Appl. Microbiol.* **94**, 580–586 (2003).
15. Somlyai, G. et al. Naturally occurring deuterium is essential for the normal growth rate of cells. *FEBS Lett.* **317**, 1–4 (1993).
16. Cong, F.S. et al. Deuterium-depleted water inhibits human lung carcinoma cell growth by apoptosis. *Exp. Ther. Med.* **1**, 277–283 (2010).
17. Kovács, A. et al. Deuterium depletion may delay the progression of prostate cancer. *J. Cancer Ther.* **2**, 548–556 (2011).
18. Somlyai, G. et al. Pre-Clinical and Clinical Data Confirm the Anticancer Effect of Deuterium Depletion. *Biomacromolecular Journal* **2**, 1–7 (2016).
19. Zhang, X., Gaetani, M., Chernobrovkin, A. & Zubarev, R.A. Anticancer Effect of Deuterium Depleted Water - Redox Disbalance Leads to Oxidative Stress. *Mol. Cell. Proteomics* **18**, 2373–2387 (2019).
20. Zhang, X., Wang, J. & Zubarev, R.A. Slight Deuterium Enrichment in Water Acts as an Antioxidant: Is Deuterium a Cell Growth Regulator? *Mol. Cell. Proteomics* **19**, 1790–1804 (2020).

21. Xie, X. & Zubarev, R.A. Isotopic Resonance Hypothesis: Experimental Verification by Escherichia coli Growth Measurements. *Sci. Rep.* **5**, 9215 (2015).
22. Marshall, A.G. et al. Protein Molecular Mass to 1 Da by 13C, 15N Double-Depletion and FT-ICR Mass Spectrometry. *J. Am. Chem. Soc.* **119**, 433–434 (1997).
23. Gallagher, K.J. et al. Isotope Depletion Mass Spectrometry (ID-MS) for Accurate Mass Determination and Improved Top-Down Sequence Coverage of Intact Proteins. *J. Am. Soc. Mass Spectrom.* **31**, 700–710 (2020).
24. Zubarev, R.A. et al. Early life relict feature in peptide mass distribution. *Cent. Eur. J. Biol.* **5**, 190–196 (2010).
25. Zubarev, R.A. Role of stable isotopes in life--testing isotopic resonance hypothesis. *Genomics Proteomics Bioinformatics* **9**, 15–20 (2011).
26. Xie, X. & Zubarev, R.A. On the Effect of Planetary Stable Isotope Compositions on Growth and Survival of Terrestrial Organisms. *PLoS One* **12**, e0169296 (2017).
27. Savitski, M.M. et al. Tracking cancer drugs in living cells by thermal profiling of the proteome. *Science* **346**, 1255784 (2014).
28. Pozzo, T., Akter, F., Nomura, Y., Louie, A.Y. & Yokobayashi, Y. Firefly Luciferase Mutant with Enhanced Activity and Thermostability. *ACS Omega* **3**, 2628–2633 (2018).
29. Khoury, G.A., Baliban, R.C. & Floudas, C.A. Proteome-wide post-translational modification statistics: frequency analysis and curation of the swiss-prot database. *Sci. Rep.* **1**, 90 (2011).
30. Zubarev, R.A., Demirev, P.A., Haakansson, P. & Sundqvist, B.U.R. Approaches and Limits for Accurate Mass Characterization of Large Biomolecules. *Anal. Chem.* **67**, 3793–3798 (1995).
31. Arnér, E.S. & Holmgren, A. Physiological functions of thioredoxin and thioredoxin reductase. *Eur. J. Biochem.* **267**, 6102–6109 (2000).
32. Lodish, H. et al. in Molecular Cell Biology. 4th edition (WH Freeman, New York; 2000).
33. Paik, S., Kim, C.-y., Song, Y.-k. & Kim, W.-s. Technology Insight: application of molecular techniques to formalin-fixed paraffin-embedded tissues from breast cancer. *Nat. Clin. Pract. Oncol.* **2**, 246–254 (2005).
34. Kevadiya, B.D. et al. Diagnostics for SARS-CoV-2 infections. *Nat. Mater.* **20**, 593–605 (2021).
35. Ishino, S. & Ishino, Y. DNA polymerases as useful reagents for biotechnology – the history of developmental research in the field. *Front. Microbiol.* **5**, 465–465 (2014).
36. Wang, Y. et al. A novel strategy to engineer DNA polymerases for enhanced processivity and improved performance in vitro. *Nucleic Acids Res.* **32**, 1197–1207 (2004).
37. Huggett, J., Dheda, K., Bustin, S. & Zumla, A. Real-time RT-PCR normalisation; strategies and considerations. *Genes Immun.* **6**, 279–284 (2005).
38. Luk, L.Y.P. et al. Unraveling the role of protein dynamics in dihydrofolate reductase catalysis. *Proc. Natl. Acad. Sci. U.S.A.* **110**, 16344-16349 (2013).

39. Luk, L.Y.P. et al. Protein Isotope Effects in Dihydrofolate Reductase From Geobacillus stearothermophilus Show Entropic–Enthalpic Compensatory Effects on the Rate Constant. *J. Am. Chem. Soc.* **136**, 17317–17323 (2014).
40. Benjamin, D.J. et al. Redefine statistical significance. *Nat. Hum. Behav* **2**, 6–10 (2018).
41. Åqvist, J., Kazemi, M., Isaksen, G.V. & Brandsdal, B.O. Entropy and Enzyme Catalysis. *Acc. Chem. Res.* **50**, 199–207 (2017).
42. Arcus, V.L. & Mulholland, A.J. Temperature, Dynamics, and Enzyme-Catalyzed Reaction Rates. *Annual Review of Biophysics* **49**, 163–180 (2020).
43. Dittwald, P., Valkenborg, D., Claesen, J., Rockwood, A.L. & Gambin, A. On the Fine Isotopic Distribution and Limits to Resolution in Mass Spectrometry. *J. Am. Soc. Mass Spectrom.* **26**, 1732–1745 (2015).
44. Seeman, J.I., Secor, H.V., Disselkamp, R. & Bernstein, E.R. Conformational analysis through selective isotopic substitution: supersonic jet spectroscopic determination of the minimum energy conformation of o-xylene. *J. Chem. Soc., Chem. Commun.*, 713–714 (1992).
45. Yergey, J., Heller, D., Hansen, G., Cotter, R.J. & Fenselau, C. Isotopic distributions in mass spectra of large molecules. *Anal. Chem.* **55**, 353–356 (1983).
46. Brauner, J.W., Dugan, C. & Mendelsohn, R. 13C Isotope Labeling of Hydrophobic Peptides. Origin of the Anomalous Intensity Distribution in the Infrared Amide I Spectral Region of β-Sheet Structures. *J. Am. Chem. Soc.* **122**, 677–683 (2000).
47. Rossi, M., Scheffler, M. & Blum, V. Impact of Vibrational Entropy on the Stability of Unsolvated Peptide Helices with Increasing Length. *J. Phys. Chem. B* **117**, 5574–5584 (2013).
48. Goethe, M., Fita, I. & Rubi, J.M. Vibrational Entropy of a Protein: Large Differences between Distinct Conformations. *J. Chem. Theory Comput.* **11**, 351–359 (2015).
49. Zoi, I. et al. Modulating Enzyme Catalysis through Mutations Designed to Alter Rapid Protein Dynamics. *J. Am. Chem. Soc.* **138**, 3403–3409 (2016).
50. Galzitskaya, O.V. Influence of Conformational Entropy on the Protein Folding Rate. *Entropy* **12**, 961–982 (2010).

Figures

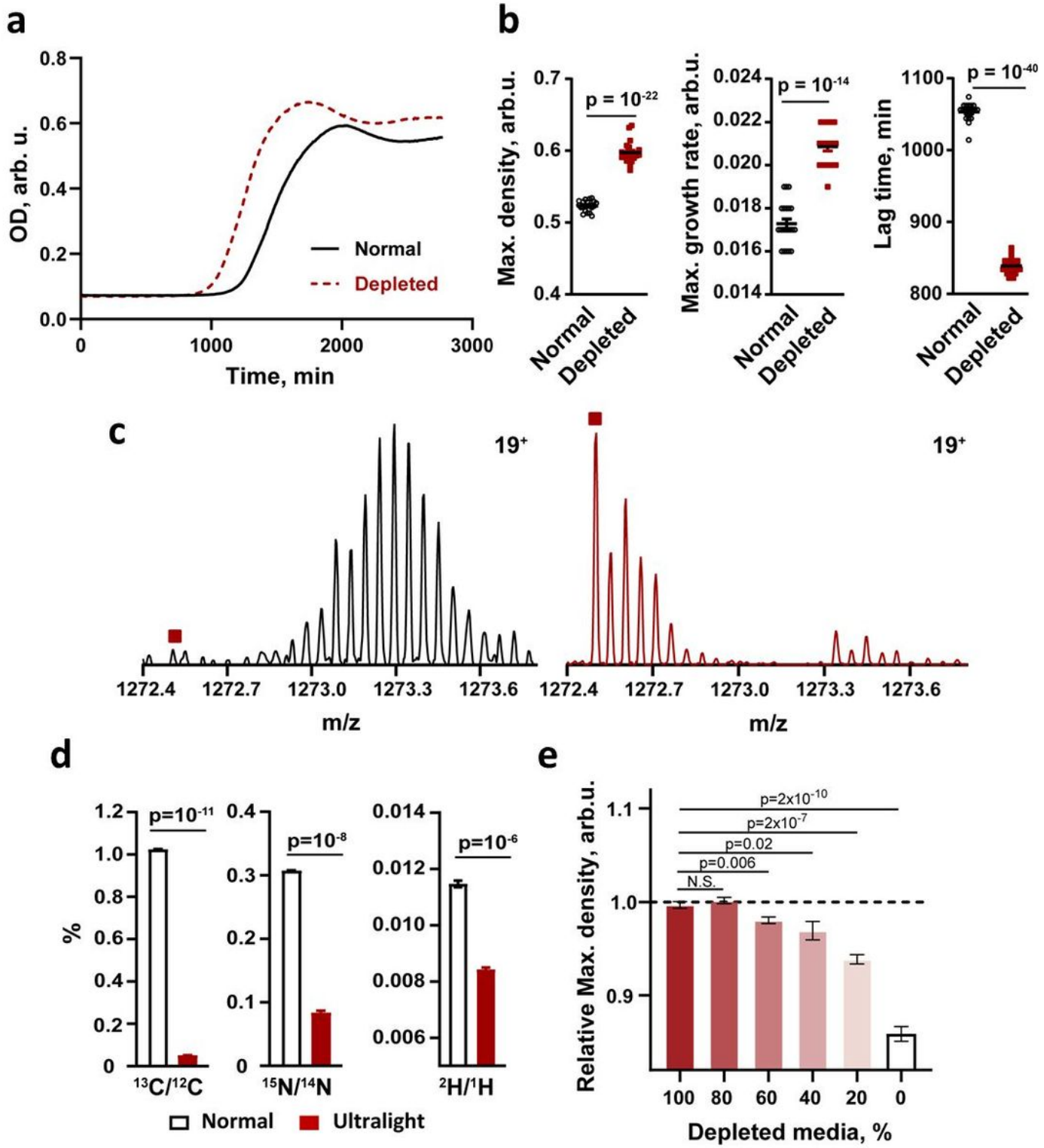

Figure 1

***E. coli* growth in Normal and Depleted media. a,** The growth curves of *E. coli* BL21 grown in Normal and Depleted M9 media (n=21). **b**, The differences in maximum density (left), maximum growth rate (middle) and lag time (right) of *E. coli* grown in Normal and Depleted media (n=21). **c**, Mass spectrum of the *E. coli* protein Stringent Starvation Protein A (24.1 kDa) grown in the Normal (left) and Depleted (right) media. The monoisotopic mass position is marked by square. **d**, FT isoR MS analysis of $^{13}C/^{12}C$ (left), $^{15}N/^{14}N$

(middle), $^{2}H/^{1}H$ (right) in *E. coli* grown in Normal and Depleted M9 media (n=3). **e**, Dose-response effect of the Depleted media dilution by the Normal media on maximum density of *E. coli* bacteria (n=8).

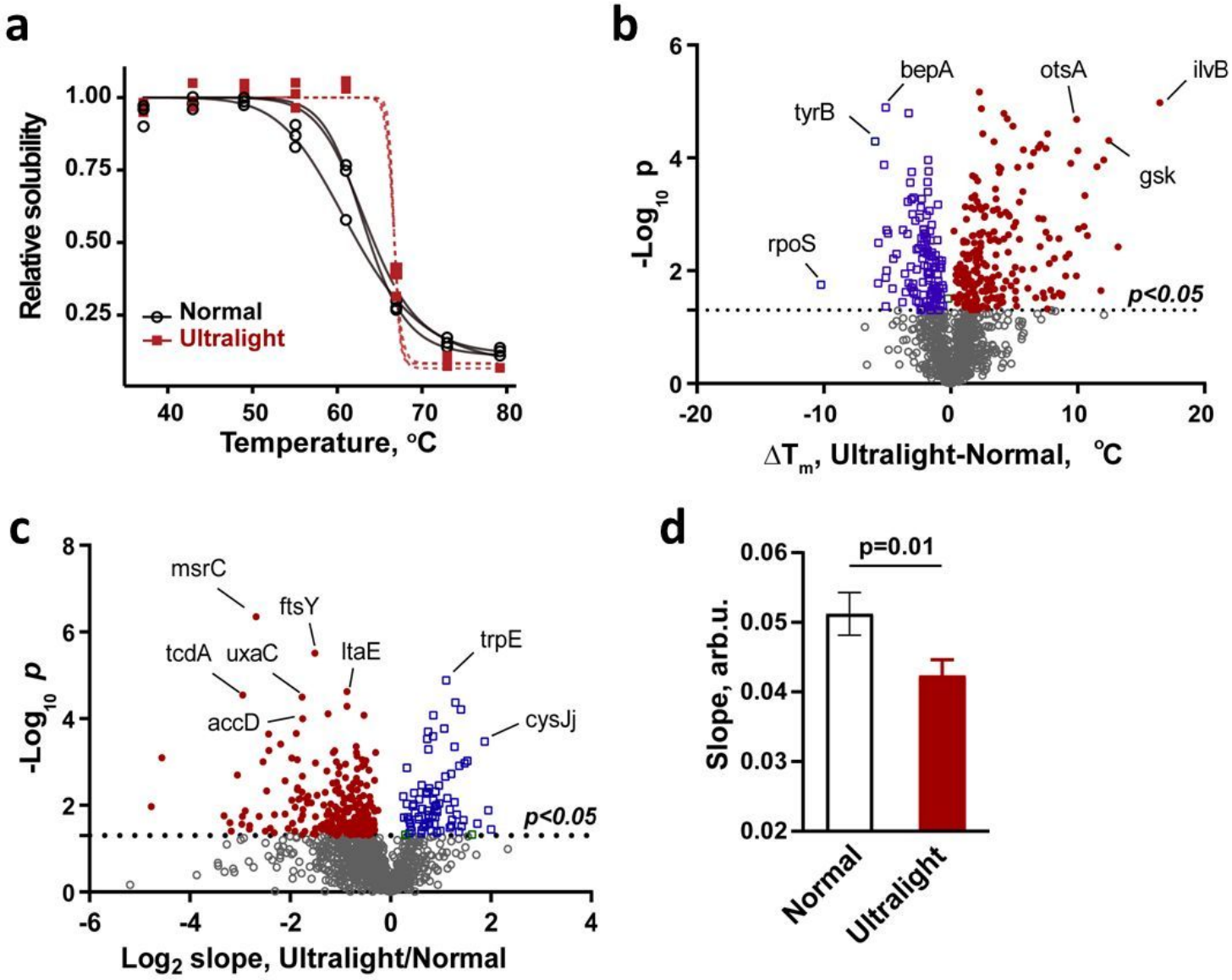

Figure 2

Thermal stability of bacterial proteins. a, The melting curves of gltB in *E. coli* BL21 grown in Normal and Depleted media (n=3). **b**, Volcano plot of melting temperature differences of proteins in *E. coli* grown in Depleted versus Normal media (median values, n=3). The horizontal line indicates the p value of 0.05 in two-tailed unpaired t-test. The proteins more stable in the Depleted media have positive ΔT_m values (red dots), while less stable proteins have negative ΔT_m values (blue dots). **c**, Volcano plot of slopes of the *E. coli* protein melting curves for bacteria grown in Depleted and Normal media (medians, n=3). The horizontal line indicates the p value of 0.05 in two-tailed unpaired t-test. The proteins from the Depleted media with steeper slopes have negative Log_2 values (red dots), while those with more shallow slopes

have positive values (blue dots). **d**, Comparison of median slopes of proteins in *E. coli* grown in Normal and Depleted media (n=3).

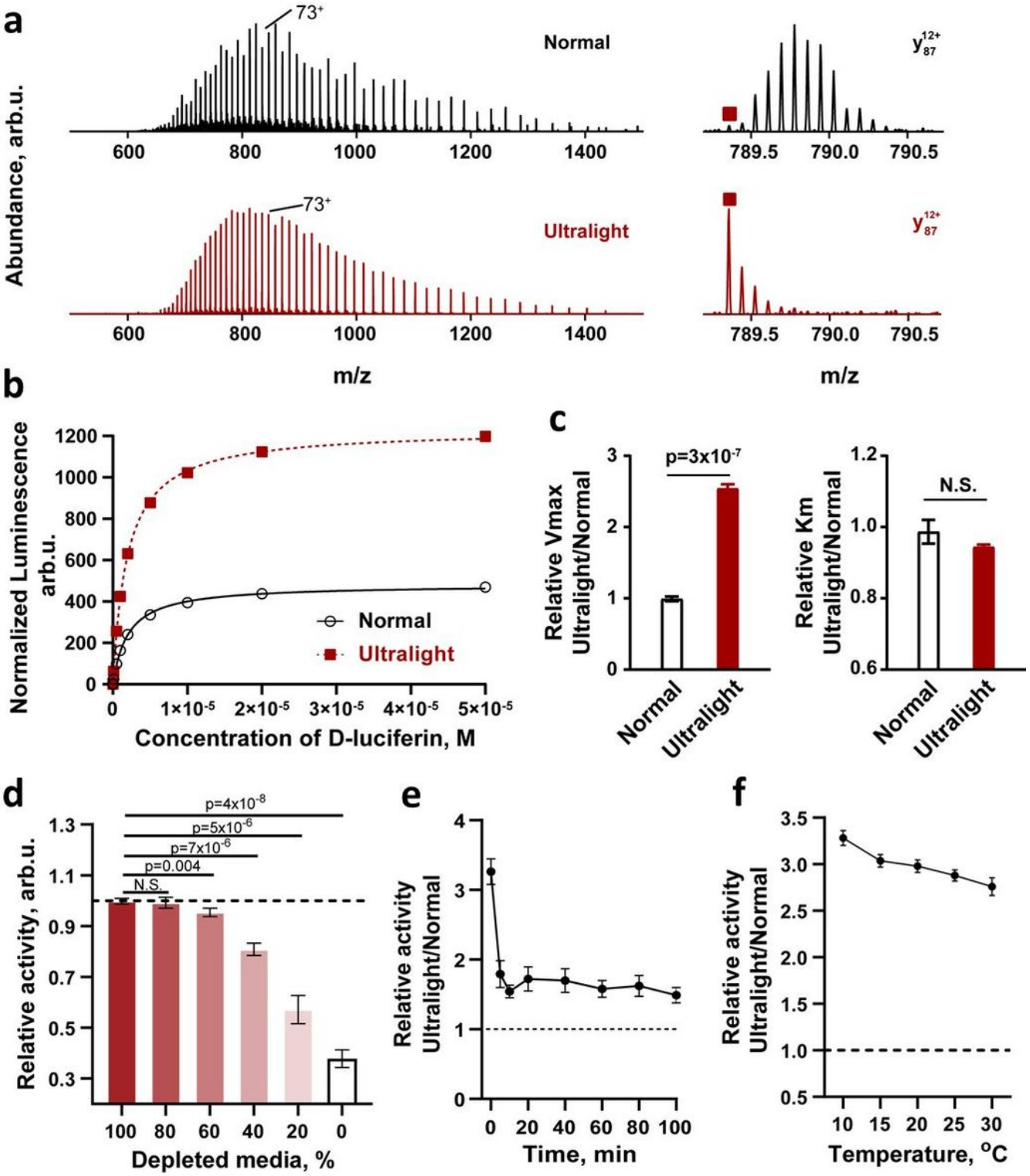

Figure 3

Analysis of luciferase YY5 fracII by mass spectrometry and activity comparison of Normal and Ultralight enzyme. a, Electrospray ionization mass spectra of fracII of Normal and Ultralight luciferase YY5 (left) and a backbone fragment obtained by MS/MS of molecular ions; square denotes monoisotopic mass. **b**, Activity curve of luciferase YY5 fracII. The luminescence readings (n=4) were normalized to the total UV absorbance in SCX chromatography before being fitted with the Michaelis-Menten equation. **c**, Kinetic parameters Vmax (left) and Km (right) of the Normal and Ultralight luciferase YY5, fracII (n=4). **d**, Dose-response effect of the Depleted media dilution by the Normal media on activity of Luciferase YY5 (n=6). **e**, The relative activity of the Ultralight luciferase YY5 fracII compared to Normal enzyme after heating at 50 °C for different time intervals and cooling to RT (n=4). **f**, The relative activity of the Ultralight luciferase YY5 fracII compared to Normal enzyme at different temperatures (n=4).

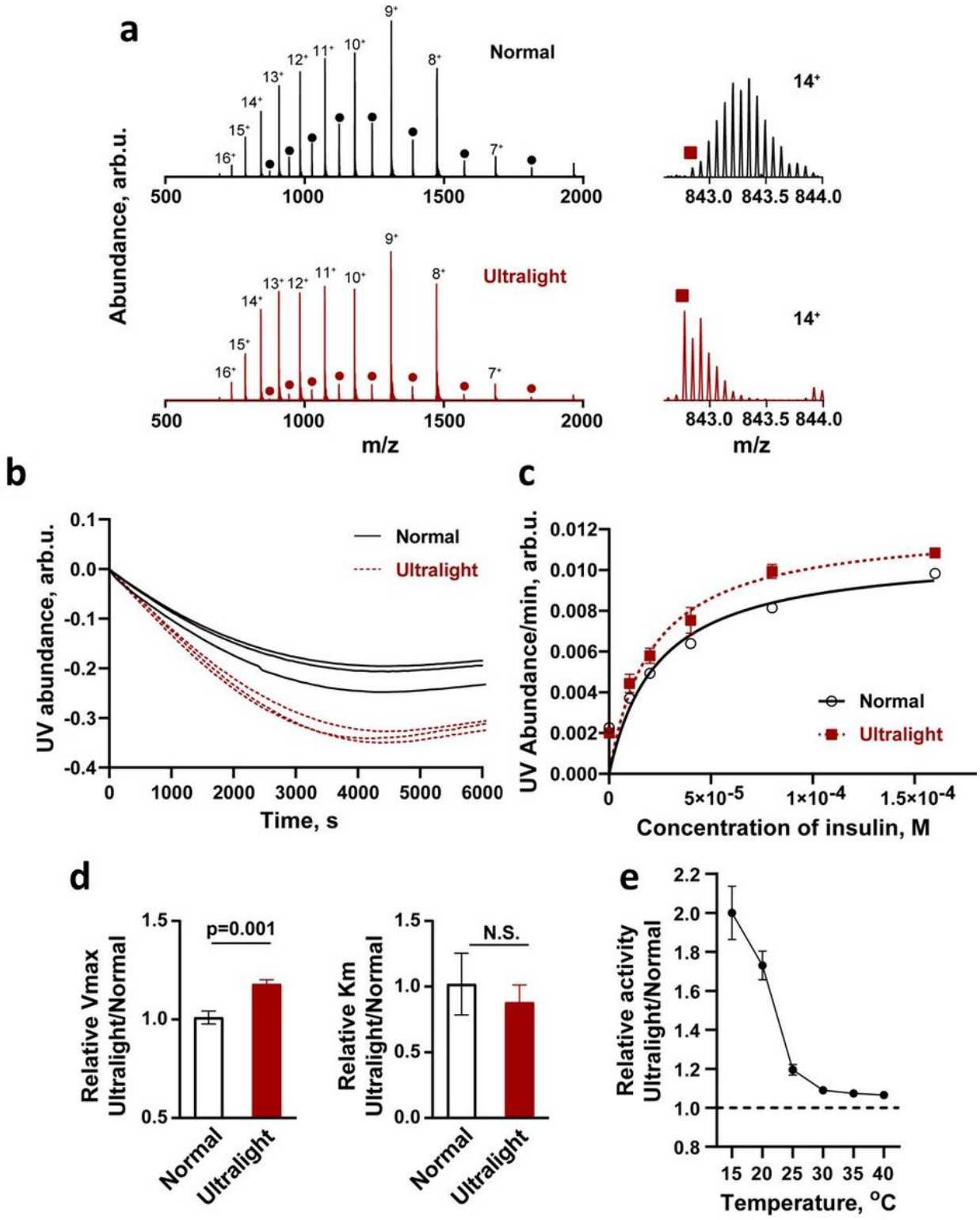

Figure 4

Analysis of Trx by mass spectrometry and activity comparison of Normal and Ultralight enzyme. a, Electrospray ionization mass spectrum of the SEC-purified Normal (top) and Ultralight (bottom) thioredoxin. The dots indicate the thioredoxin dimer, squares - the monoisotopic masses. **b**, Activity comparison of Normal and Ultralight thioredoxin (n=3). **c**, Kinetic curves of the Normal and Ultralight thioredoxin (n=3). **d**, The kinetic parameters Vmax (left) and Km (right) of the Normal and Ultralight

thioredoxin (n=3). **e**, The relative activity of the Ultralight thioredoxin compared to Normal enzyme at different temperatures (n=4).

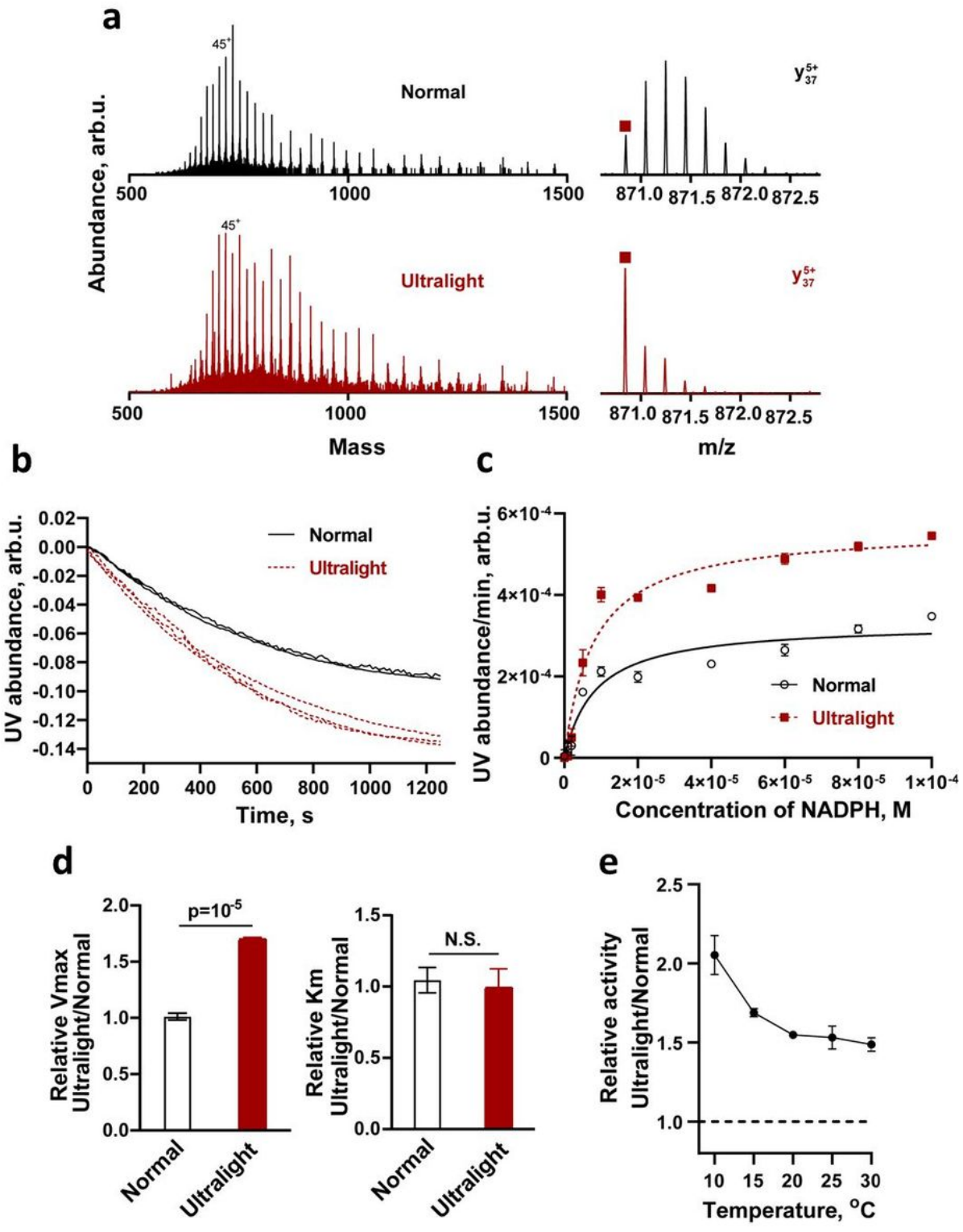

Figure 5

Analysis of BsDHFR by mass spectrometry and activity comparison of Normal and Ultralight enzyme. a, Electrospray ionization mass spectra of Normal and Ultralight BsDHFR (left) and a backbone fragment

obtained by MS/MS of molecular ions; square - the monoisotopic mass. **b**, Activity comparison of Normal and Ultralight BsDHFR (n=3). **c**, Kinetic curves of the Normal and Ultralight BsDHFR (n=4). **d**, The kinetic parameters Vmax (left) and Km (right) of the Normal and Ultralight BsDHFR (n=4). **e**, The relative activity of the Ultralight tBsDHFR compared to Normal enzyme at different temperatures (n=3).

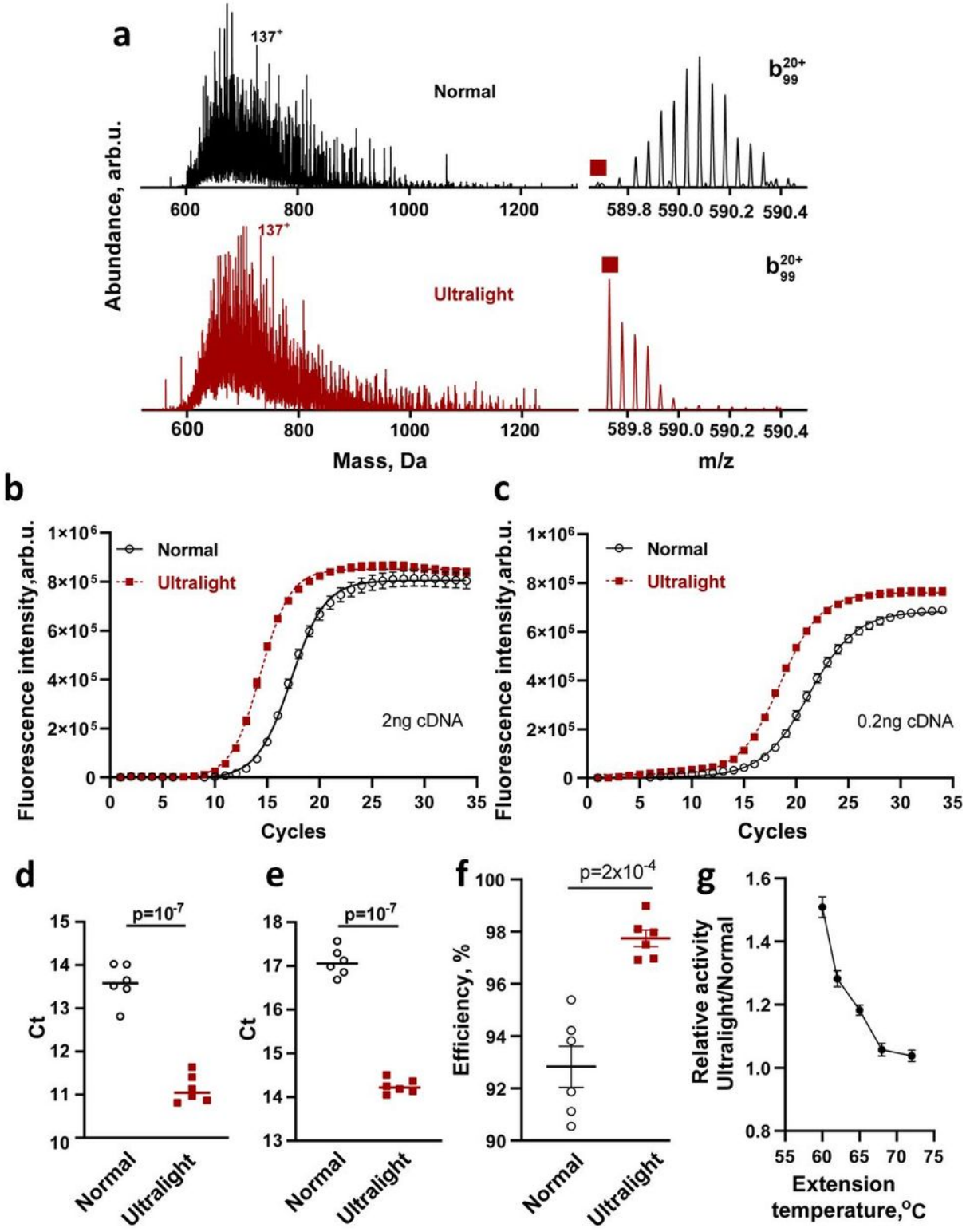

Figure 6

Analysis of Pfu by mass spectrometry and activity comparison of Normal and Ultralight enzyme. a, Electrospray ionization mass spectra from SEC of Normal and Ultralight Pfu (left) and a backbone fragment obtained by MS/MS of molecular ions; square - the monoisotopic mass. **b**, **c**, Comparisons of the RT PCR analyses with 2 ng and 0.2 ng template cDNA catalyzed by Normal or Ultralight Pfu (n=6). **d**, **e**, Comparisons of the corresponding Ct values. **f**, Efficiency of PCR with Normal and Ultralight Pfu (n=6). **g**, The relative activity of the Ultralight Pfu compared to Normal enzyme at different temperatures (n=3).

Supplementary Files

This is a list of supplementary files associated with this preprint. Click to download.

- SupplementaryTable1.xlsx
- SupplementaryTable2.xlsx
- SupportingInformationDec62021.docx